# Nonmonotonic crossover from adsorption to desorption in supercritical fluid near a weakly attractive surface

Alla Oleinikova* and Ivan Brovchenko
*Physical Chemistry, Dortmund University of Technology, Otto-Hahn-Strasse 6, Dortmund, D-44227, Germany*
(Received 27 June 2008; published 2 December 2008)

The density profiles of a supercritical Lennard-Jones fluid near a weakly attractive surface are used to study the excess adsorption $\Gamma$ of supercritical fluid in a wide density range. We report the observation of two extrema of $\Gamma$ along the isotherm as a function of density. The attractive fluid-wall interaction potential tends to make $\Gamma$ positive, whereas the missing neighbor effect tends to make $\Gamma$ negative. The latter effect enhances with increasing fluid density due to the growth of the fluid-fluid attraction that results in the crossover from adsorption to depletion ($\Gamma=0$) at some particular fluid density. With approaching the critical point, $\Gamma$ decreases as the bulk correlation length and passes through a minimum when the average density of confined fluid is close to the bulk critical density. Variation of $\Gamma$ with temperature and density is determined by the monotonic trend from adsorption to desorption upon increasing fluid density and by the increase of the absolute value of $\Gamma$ when approaching the critical point. Interplay of these trends results in two extrema of $\Gamma$ in the temperature-density plane. This effect may be responsible for the crossover from adsorption to desorption with approaching the critical temperature observed experimentally along the isotherms and along the critical isochore. The density profiles of a supercritical fluid are found to be exponential and the power law behavior predicted theoretically was not detected even when the bulk correlation length $\xi$ achieves 11 molecular diameters.

DOI: 10.1103/PhysRevE.78.061601 PACS number(s): 68.08.−p, 05.70.Jk, 64.70.F−

## I. INTRODUCTION

Adsorption of fluids at surfaces is involved in various industrial applications. A renewed interest to this phenomena is provoked by the urgent necessity to reduce concentration of carbon dioxide in Earths atmosphere. Injection of $CO_2$ into porous geological formations is currently considered the most promising long-term storage aiming to mitigate global warming. The efficiency of the storage strongly depends on the interaction of injected fluid with pore surface, as well as on temperature and pressure. As a supercritical fluid phase is the main storage form, establishing of the regularities of the supercritical adsorption common for various systems is an important challenge.

The effect of the critical fluctuations on various fluid properties spreads far away from the critical point. Therefore, many previous studies of adsorption of supercritical fluids were focused on the phenomenon of critical adsorption predicted by Fisher and de Gennes [1]. With approaching the critical temperature $T_c$ along the bulk critical isochore, the excess adsorption $\Gamma$ of fluids at the surface should demonstrate the power-law divergence

$$\Gamma(\tau) \sim \tau^{\beta-\nu}, \tag{1}$$

where $\tau=(T/T_c-1)$, $\beta\approx 0.326$ and $\nu\approx 0.63$ are the universal critical exponents [2]. Such behavior is expected in the limit of the infinitely strong surface attraction which completely suppresses the effect of missing neighbors. In this case, the density profile $\rho(z)$ of a fluid near a surface should be described by the universal scaling function $P(x)$

$$\rho(z) \sim \tau^{\beta} P(z/\xi), \tag{2}$$

which has the following asymptotic limits:

$$P(x \to 0) \sim x^{-\beta/\nu}, \tag{3}$$

$$P(x \to \infty) \sim e^{-x}. \tag{4}$$

Renormalization group approach yields additional (weaker) singularities in $P(x\to 0)$ [3,4], whereas higher-order exponential terms may appear in $P(x\to\infty)$ [5]. Various crossover equations, which incorporate two asymptotic behaviors (3) and (4), were proposed and applied for description of the experimental data for binary mixtures [5–7]. One of the most widely used crossover equation has been proposed by Liu and Fisher [5]:

$$P(z/\xi) = (\xi/z + c)^{\beta/\nu} \exp\left(-\frac{z}{\xi}\right), \tag{5}$$

where parameter $c$ controls crossover from the power-law to the exponential behavior and it is expected to be universal since $P(x\to\infty)=P(x\to 0)c^{\beta/\nu}$. Various theoretical approaches yield the value of $c$ close to 1 (see Ref. [6], for example).

Most of the available experimental data corresponding to the case of a strong adsorption in binary mixtures were found to be consistent with the crossover equation (5), although the microscopic correction to the distance $z$ should be introduced in this case in order to ensure a finite value of the concentration at the wall. The value of $c$ obtained from these fits is extremely sensitive to the details of the fitting procedure and was often found notably larger than 1 [8], so that the power-law regime could not be unambiguously detected [8,9]. The asymptotic temperature dependence of the excess adsorption $\Gamma$ along the critical isochore in binary mixtures was often found to be consistent with Eq. (1) [10,11]. However, a di-

*alla@pc2a.chemie.uni-dortmund.de

 

vergence stronger than the theoretically predicted $\sim\tau^{-0.3}$ was also reported [9]. In the regime of a strong adsorption, a specific "dead" fluid film with a thickness of one to several monolayers is frequently formed at the surface. The properties of this film differ notably from those of the rest of a fluid, that complicates the analysis of the concentration profiles [12,13]. Note finally, that the temperature dependence of the excess adsorption $\Gamma$ in binary mixtures of noncritical concentration shows power-law behavior, which is not yet understood theoretically [12].

The regime of weak adsorption has been much less studied theoretically and experimentally. In this case, the density (concentration) profile is nonmonotonic and possesses a maximum at some distance from the surface due to the domination of a missing neighbor effect [14,15]. The available experimental studies of the weak adsorption in binary mixtures [16] seem to be consistent with the theoretically predicted nonmonotonic concentration profiles. Scaling theory [17] predicts a weak divergence of $\Gamma$ with the crossover to the behavior described by Eq. (1) very close to the critical point. The experimental studies of the temperature dependence of $\Gamma$ in binary mixtures are rare [18] and not well understood.

Although the critical adsorption of net (one-component) fluids was studied extensively by various experimental techniques, this phenomenon remains even less understood than that in binary mixtures [19]. Both critical adsorption (positive $\Gamma$) [20–22] and critical desorption (negative $\Gamma$) [20,23] were reported close to the critical point. A behavior described by Eq. (1) is in agreement with some experimental data [22]. Some other experimental observations of the critical adsorption and critical desorption were discarded later and no experimental evidences for the critical anomaly were found (see Ref. [19] for review and discussions). A nonmonotonic temperature dependence of $\Gamma$ with a crossover from positive to negative values with the approaching the critical point reported in Refs. [20,23] has provoked numerous theoretical and computer simulation studies of adsorption in model pores [24–27]. A convincing physical explanation for the crossover from critical adsorption to critical desorption is still missing, however.

Recent simulation studies of the critical behavior of subcritical fluid ($T<T_c$) near a weakly attractive surface evidence nonmonotonic dependence of the excess adsorption and a crossover from adsorption to desorption in a vapor phase when approaching the critical point [28]. Later, rather similar behavior was reported for the experimentally studied adsorption of propane in a silica aerogel along the supercritical isotherms [29].

In the present paper, we study the density profiles of supercritical Lennard-Jones (LJ) fluids near a weakly attractive wall along the critical isotherm and several pore isochores in order to find regularities of the excess adsorption $\Gamma$ in a wide density range. We show that in a wide thermodynamic range the effect of missing neighbors dominates the fluid-surface attraction and $\Gamma$ is negative and proportional to the correlation length $\xi$. We analyze applicability of the available theory [Eqs. (1)–(5)] to describe adsorption and desorption of a fluid near a surface. We have found a thermodynamic state with zero excess adsorption. The location of the line $\Gamma=0$ in the temperature-density plane for fluids near surfaces is analyzed and its relation to the experimentally observed crossover from adsorption to desorption [20,23,29] upon varying temperature or density is discussed.

## II. METHODS

We studied a LJ fluid, having an interparticle interaction of the form

$$U_{LJ}(r) = 4\epsilon[(\sigma/r)^{12} - (\sigma/r)^6], \tag{6}$$

where $\epsilon$ measures the well depth of the potential, while $\sigma$ sets the length scale. The potential was spherically truncated at a radius $2.5\sigma$ and left unshifted. No long-range corrections were applied to account for effects of the truncation. The bulk liquid-vapor coexistence curve of this LJ fluid was studied in detail and its critical temperature and density were accurately located [30,31]. A LJ fluid was confined in the slit pores of width $H=12$ and $40\sigma$ with structureless weakly attractive walls. Each planar surface comprises of a single plane of LJ molecules and interacts with a fluid molecule via the long-range potential of a form

$$U_w(z) = 4\epsilon f[0.4(\sigma/z)^{10} - (\sigma/z)^4], \tag{7}$$

where factor $f$ determines the relative strength of fluid-wall and fluid-fluid interactions and was set equal to 0.3 in the present simulations. No truncation was applied to $U_w(z)$.

The average density of the LJ fluid confined in a pore may be calculated based on the pore volume accessible for LJ molecules. The fluid-wall interaction described by Eq. (7) is equal to zero at a distance $0.86\sigma$ from the pore wall and so in an operational approach this interval could be divided equally between the volumes of the fluid and the solid. From the analysis of the density and order parameter profiles, the volume inaccessible for fluid molecules was found slightly larger, i.e., a slab of $0.55\sigma$ width near a pore wall should be attribute to the volume of a solid [28,31,32]. As a result, the volume accessible for the centers of molecules is reduced with respect to the volume calculated simply using the pore width $H$ by a factor of about 1.028 for $H=40\sigma$ and 1.101 for $H=12\sigma$. Throughout the paper we use the average pore density $\rho_{\mathrm{av}}$ accounted for the correction on the accessible volume. Accordingly, we use $\Delta z=z-0.55\sigma$ as a reasonable measure of the distance of molecules to the surface.

The phase diagrams of the confined LJ fluids were determined using Monte Carlo (MC) simulations in the Gibbs ensemble in Refs. [31,32]. The density profiles of the LJ fluid in pores were studied in various supercritical states. The bulk critical temperature $T_c=1.1876$ (temperature of LJ fluid is scaled by $\epsilon/k_B$, where $k_B$ is the Boltzmann's constant) and the bulk critical density $\rho_c\approx 0.32\sigma^{-3}$ of the studied LJ fluid were determined using a histogram reweighting method with subsequent mixed-field finite size scaling [30]. Very close critical parameters were obtained from the fit of the order parameter to the simple scaling law and from the linear fit of the diameter of the coexistence curve [31]. The latter approach used for the estimation of the pore critical density (average pore density at the pore critical temperature) gives $\rho_{\mathrm{av}}=0.262\sigma^{-3}$ and $0.281\sigma^{-3}$ in the pores of width $H=40$ and

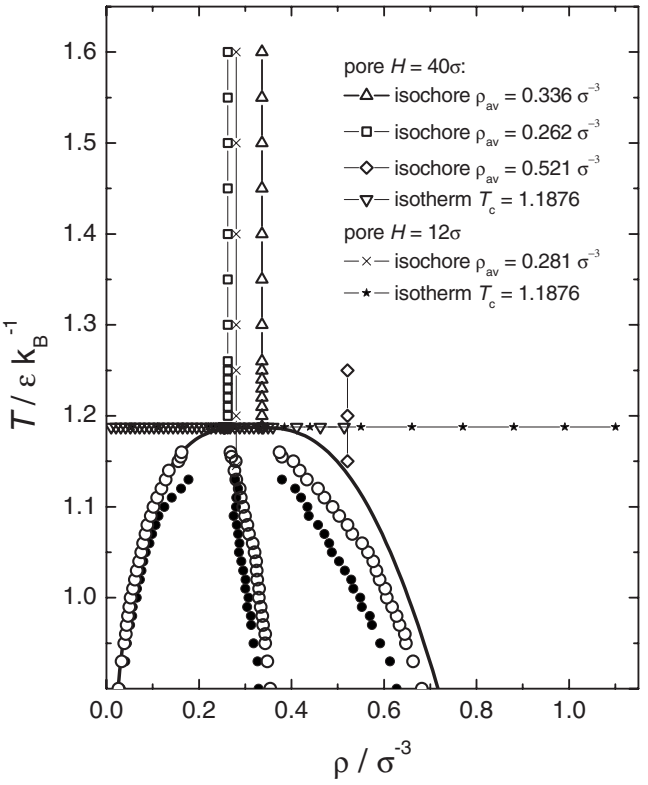


FIG. 1. Location of the thermodynamic state points, where the density profiles and the excess adsorption of a LJ fluid in slit pores with weakly attractive walls were studied, with respect to the bulk liquid-vapor coexistence curve (thick solid line) and the liquid-vapor coexistence curves (the average densities of the coexisting phases and the diameters) of a LJ fluid in the pores of width $H=12\sigma$ (closed symbols) and $H=40\sigma$ (open symbols). The parameters of the studied isotherm and isochores are indicated in the figure.

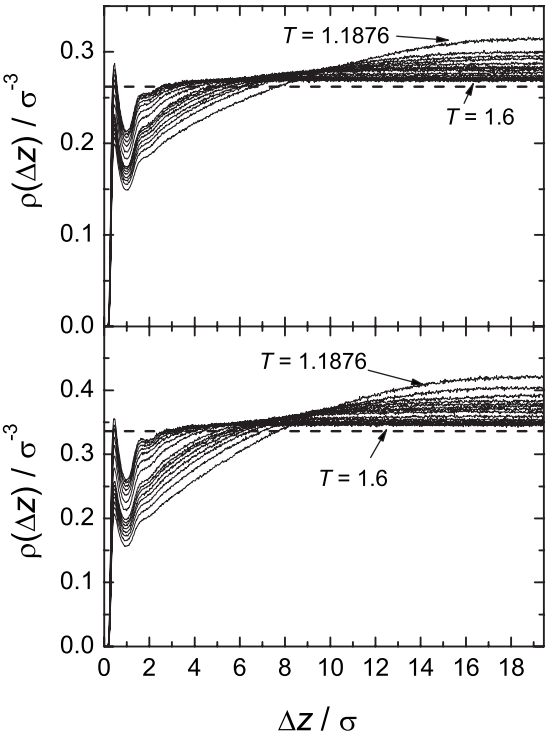


FIG. 2. The density profiles $\rho(\Delta z)$ of a LJ fluid in the slit pore with $H=40\sigma$ along the pore critical isochore $\rho_{av}=0.262\sigma^{-3}$ (upper panel) and along the isochore $\rho_{av}=0.336\sigma^{-3}$ (lower panel), indicated by the horizontal dashed lines.

$12\sigma$, respectively [31,32]. In both pores, the density profiles were studied in the thermodynamic states along the critical isotherm at $T=T_c=1.1876$ and along the isochores with the pore critical densities given above. In addition, the states at two additional isochores with the average densities $\rho_{av}=0.336$ and $0.521\sigma^{-3}$ were studied for larger pore with $H=40\sigma$. The thermodynamic state points studied are shown in Fig. 1 together with the phase diagrams of bulk and confined LJ fluids.

The density profiles were obtained by constant volume MC simulations. The strong density gradient normal to the pore wall makes the reliable determination of the density profiles in the pore with $H=40\sigma$ very time consuming. This problem was partially overcome by using two kinds of the moves in MC simulations. In addition to the standard short-range MC moves with a maximal displacement of a molecule, which provides an acceptance probability of about 50%, we used long-distance molecular transfer inside the simulation cell: an attempt to place randomly chosen fluid molecule into randomly chosen position in the cell. The latter MC move is similar to the one used in Gibbs ensemble simulations for molecular transfers between the two simulation boxes. The acceptance probability of these MC moves varied from a few percent at high densities to about 50% at low densities. Such long-distance molecular transfers essentially improve the sampling of the density profiles. The kind of a MC move was chosen randomly with probability 50%. The local density was determined for layers of $0.02\sigma$ width and the resulting density profiles were averaged over $2\times10^5$ configurations taken each 5000th MC step. This yielded a statistical uncertainty of the local density less than 1%.

## III. RESULTS

### A. Pore isochores

The density profiles $\rho(\Delta z)$ of a LJ fluid in the slit pore of width $H=40\sigma$ at 15 temperatures in the range $1.1876\leqslant T\leqslant1.60$ along the pore critical isochore $\rho_{av}=0.262\sigma^{-3}$ and along the isochore $\rho_{av}=0.336\sigma^{-3}$ are shown in Fig. 2. The density gradient is the largest at the bulk critical temperature $T_c=1.1876$. Upon heating, this gradient continuously decreases and the fluid density in the pore interior approaches the average pore density. In the case of $\rho_{av}=0.262\sigma^{-3}$, the density in the pore interior exceeds $\rho_{av}$ by about 16% at $T=T_c$ and by just 3% at $T=1.6$. In the case of $\rho_{av}=0.336\sigma^{-3}$, increase of the density in the pore interior is even stronger: it rises up to 25% at the critical temperature. The drop of the density in the pore interior is sharp, when the temperature rises from $T_c$ on about 1–2 %, and is essentially weaker at higher temperatures.

The density profiles shown in Fig. 2 show gradual change moving away from the pore wall when $\Delta z$ exceeds about $2\sigma$. At shorter distances, notable density oscillations are present

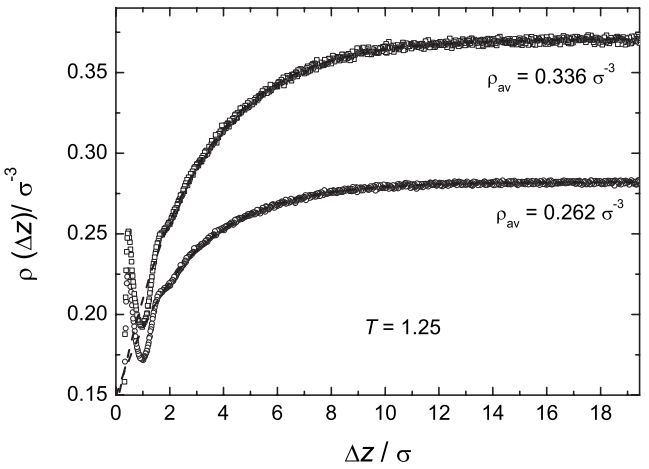


FIG. 3. The density profiles $\rho(\Delta z)$ of a LJ fluid in the pore with $H=40\sigma$ at $T=1.25$ and two average pore densities, indicated in the figure, and their fits to the exponential equation (8) in the range $\Delta z \geqslant 2\sigma$ (dashed lines).

at all temperatures. The first maximum of $\rho(\Delta z)$ reflects localization of molecules in the fluid-wall potential well, whereas the second (much weaker) density maximum is caused by the localization of molecules in the potential well caused by the molecules localized in the first layer. The nonmonotonic part of the density profiles $\rho(\Delta z)$ within the distance of $2\sigma$ from the wall was excluded from the analysis and the remaining gradual part of the density profiles was fitted to the exponential equation

$$\rho(\Delta z) = \rho_b - (\rho_b - \rho_s)\exp\left(-\frac{\Delta z}{\xi}\right), \tag{8}$$

where $\rho_b$ is the asymptotic fluid density far from the surface, $\rho_s$ is the density value right at the pore wall, and $\xi$ is the correlation length of a confined fluid. This equation is a modification of Eq. (4) for the case of a fluid density depletion in the asymptotic regime $z/\xi \gg 1$. Examples of the fits of $\rho(\Delta z)$ to Eq. (8) for $T=1.25$ at two average pore densities shown in Fig. 3 evidence a perfectness of the fits in the range $z > 2\sigma$. Obviously, the local density approaches $\rho_b$ exponentially without any signature of the power-law behavior, which may be expected in the asymptotic regime $z/\xi \ll 1$ [Eq. (3)] and for the long-range fluid-wall potential when $z/\xi \gg 1$ [33].

The density profiles were also fitted to the equation

$$\rho(\Delta z) = \rho_b - a_0(\xi/z + c)^{\beta/\nu}\exp\left(-\frac{z}{\xi}\right), \tag{9}$$

which is Eq. (5) modified for the case of a fluid density depletion. We have never observed improvement of the fits when using Eq. (9) instead of Eq. (8). Moreover, the values of the parameters $\xi$ and of $\rho_b$ obtained from the fits were almost identical in both cases. Accordingly, the parameter $c$ was much larger than 1, that indicates negligible role of the critical power-law term in Eq. (9).

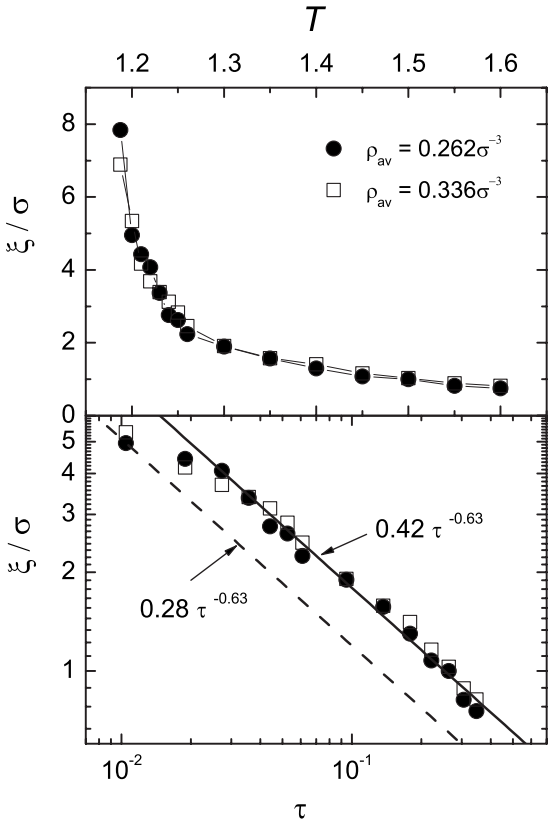


FIG. 4. Temperature dependences of the correlation length $\xi$ obtained from the fits of the fluid density profiles in the states along the pore critical isochore $\rho_{av}=0.262$ and along the isochore $\rho_{av}=0.336\sigma^{-3}$ in the pore with $H=40\sigma$ (upper panel). Dependence of $\xi$ on the reduced temperature $\tau$ in a double logarithmic scale (lower panel). Temperature dependence of the correlation length $\xi$ of a LJ fluid in a liquid phase along the pore coexistence curve [32] (dashed line) and a power law (10) with $\xi_0^+=0.42\sigma$ (solid line).

The correlation length $\xi$ obtained from the fits increases drastically, when temperature approaches the critical point (Fig. 4, upper panel). Interestingly, the fitting values of $\xi$ are very close in pores with different average pore densities $\rho_{av}=0.262$ and $0.336\sigma^{-3}$. To examine the temperature dependence of $\xi$, it is reasonable to consider the temperature distance $\tau=(T/T_c-1)$ to the critical temperature $T_c$ rather than $T$ itself. The obtained dependences of $\xi(\tau)$ are shown in a double logarithmic scale in the lower panel of Fig. 4. In the case of a bulk critical isochore, the following asymptotic behavior of the correlation length is expected:

$$\xi(\tau) = \xi_0^+\tau^{-\nu}. \tag{10}$$

The temperature dependence of $\xi(\tau)$ shown in Fig. 4 seems to be consistent with a power law (10) with the amplitude $\xi_0^+ \approx 0.42\sigma$ in the temperature range $\tau \geqslant 0.03$ (see solid line in the lower panel of Fig. 4). Closer to the critical temperature ($\tau < 0.03$), the correlation length $\xi$ obtained from the density profiles is clearly underestimated due to the effect of the second (opposite) wall. Along the bulk coexistence curve, the dependence $\xi(\tau)$ is similar to Eq. (10), but the amplitude $\xi_0^-$ is expected to be smaller by a factor of about

1.95 [2]. In fact, the power law (10) with the amplitude $0.28\sigma$ was found in the liquid phase along the pore coexistence curve in the same pore of width $H=40\sigma$ (Fig. 4, dashed line) [32]. The ratio $\xi_0^+/\xi_0^- \approx 1.5$ obtained in simulations is notably below the theoretical value of about 1.95 [2].

The obtained density profiles allow evaluation of the excess adsorption of a LJ fluid near a surface. The excess adsorption $\Gamma$ describes the excess or deficit of mass per unit surface area and can be calculated from the density profiles $\rho(\Delta z)$

$$\Gamma = \int_0^\infty [\rho(\Delta z) - \rho_b] d(\Delta z). \tag{11}$$

In the case of a slit pore, the upper limit of the integral in Eq. (11) should not exceed half of the pore width and $\Gamma$ may be obtained from the equation

$$\Gamma = \int_0^{H^*/2} \rho(\Delta z) d(\Delta z) - \rho_{\text{in}} H^*/2, \tag{12}$$

where $\rho_{\text{in}}=\rho(H^*/2)$ is the density in the pore interior and $H^*/2=H/2-0.55\sigma$ is a half of the pore width accessible for a fluid. For the calculations of the excess adsorption $\Gamma$, the value $\rho_{\text{in}}$ was determined as the average density in the fluid layer of $1\sigma$ width in the pore center. The temperature dependences of $\Gamma$ obtained by Eq. (12) using the fluid density profiles in the pore of width $H=40\sigma$ along two pore isochores are shown in the upper panel of Fig. 5. The adsorption is negative and $\Gamma$ shows apparent "divergence" when approaching the bulk critical temperature $T=1.1876$ upon cooling. Absolute value of $\Gamma$ at the average pore density $\rho_{\text{av}}=0.336\sigma^{-3}$ is notably larger than that observed at $\rho_{\text{av}}=0.262\sigma^{-3}$, indicating that thermodynamic states in the former case are closer to the bulk critical isochore.

To examine the character of the temperature dependence of $\Gamma$, it is reasonable to use the reduced temperature $\tau$ and the corresponding dependences $\Gamma(\tau)$ are shown in a double logarithmic scale in the lower panel of Fig. 5. Not very close to the critical point ($\tau \geqslant 0.03$), $\Gamma$ follows roughly a power law for the bulk correlation length (10) with the critical exponent $\nu \approx 0.63$ (solid lines). Closer to the critical point ($\tau < 0.03$), $\Gamma$ shows a trend toward saturation due to confinement, quite similar to those seen in other confined systems [25,34]. Note, that the trend of $\Gamma$ toward saturation occurs simultaneously with the deviation of the temperature dependence of the correlation length $\xi$ from the power law behavior (see lower panel in Fig. 4).

To study the effect of the pore size on the temperature dependence of the excess adsorption, the density profiles $\rho(\Delta z)$ of a LJ fluid were calculated in essentially smaller slit pore ($H=12\sigma$) in the thermodynamic states along the pore critical isochore $\rho_{\text{av}}=0.281\sigma^{-3}$ [31]. At high temperature ($T=1.6$), the profile $\rho(\Delta z)$ is almost flat in the pore interior and the density near the surface is the largest (see Fig. 6). Upon cooling, the density gradient normal to the pore wall increases and it is the strongest at the pore critical temperature $T=1.145$. Interestingly, that density profiles cross in a common point at the distance $\Delta z \approx 2.75\sigma$ from the surface, i.e., at the half distance between the wall and the pore center (see Fig. 6).

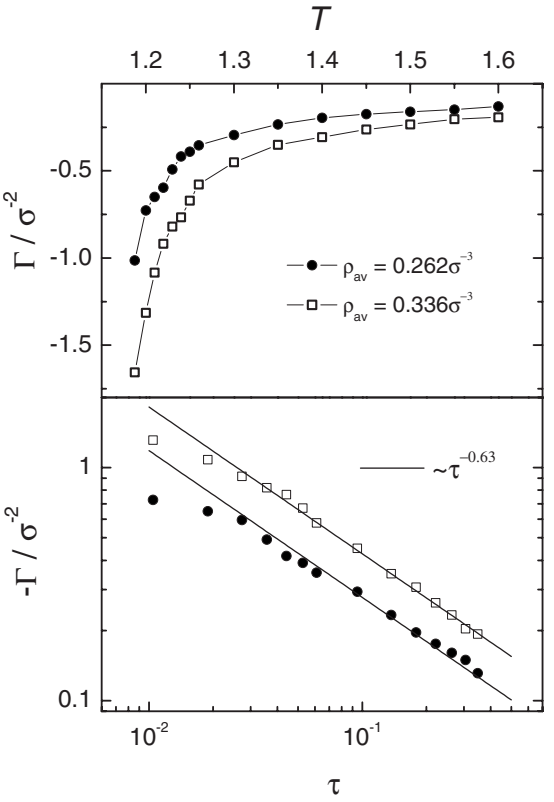


FIG. 5. Temperature dependence of the excess adsorption $\Gamma$ along the pore critical isochore $\rho_{\text{av}}=0.262$ and along the isochore $\rho_{\text{av}}=0.336\sigma^{-3}$ in the pore of width $H=40\sigma$ (upper panel). The absolute values of $\Gamma$ as a function of the reduced temperature in a double logarithmic scale (lower panel). A power law which may be agreed with the simulated dependences $\Gamma(\tau)$ not very close to the critical temperature is shown by the solid line.

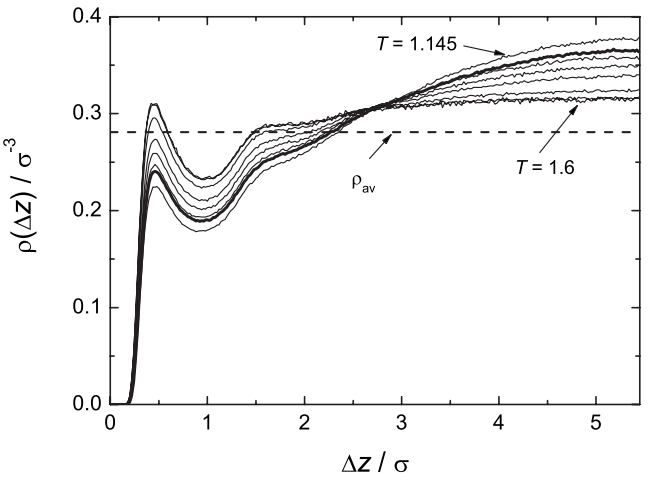


FIG. 6. Density profiles $\rho(\Delta z)$ of a LJ fluid in the slit pore with $H=12\sigma$ in the thermodynamic states along the pore critical isochore $\rho_{\text{av}}=0.281\sigma^{-3}$, indicated by the horizontal dashed line. The density profile at the bulk critical temperature is marked by the thick line.

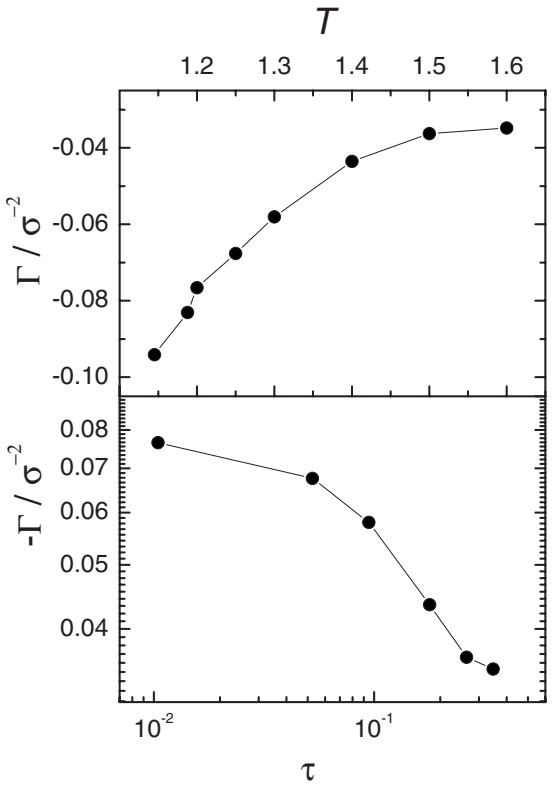


FIG. 7. Temperature dependence of the excess adsorption $\Gamma$ in the thermodynamic states along the pore critical isochore $\rho_{av}=0.281\sigma^{-3}$ in the pore of width $H=12\sigma$ (upper panel). The absolute value of $\Gamma$ as a function of the reduced temperature in a double logarithmic scale (lower panel).

The density profiles shown in Fig. 6 may be satisfactorily described by the exponential equation (8) in the range $\Delta z > 1\sigma$ at high temperatures. Close to the pore critical temperature, the shape of the gradual portion of $\rho(\Delta z)$ deviates from the exponential one due to the influence of the second (opposite) pore wall [31]. Numerical integration of the density profiles yields excess adsorption $\Gamma$ shown in Fig. 7. Similarly to the case of the larger pore (Fig. 5), $\Gamma$ shows a trend toward saturation with approaching the critical temperature. However, the power law part of the dependence $\Gamma(\tau)$ can be hardly distinguished.

### B. Critical isotherms

The density profiles of a LJ fluid in the pore of width $H=40\sigma$ calculated at various average pore densities $\rho_{av}$ from 0.005 to $0.51\sigma^{-3}$ at the bulk critical temperature $T=1.1876$ are shown in Fig. 8. These profiles possess an extended flat portion in the pore interior at low and high $\rho_{av}$, whereas a strong density gradient affects even a fluid near the pore center, when $\rho_{av}$ is close to the pore critical density $0.262\sigma^{-3}$. Similarly to the pore isochores, $\rho(\Delta z)$ may be perfectly fit to Eq. (8) for $\Delta z \geqslant 2\sigma$ and some of such fits are shown in Fig. 9. The fitting curves corresponding to Eqs. (8) and (9) are undistinguishable. This agrees with the extremely large fitting values of $c$ and evidences negligible deviations of the density profiles from the asymptotic exponential behavior of

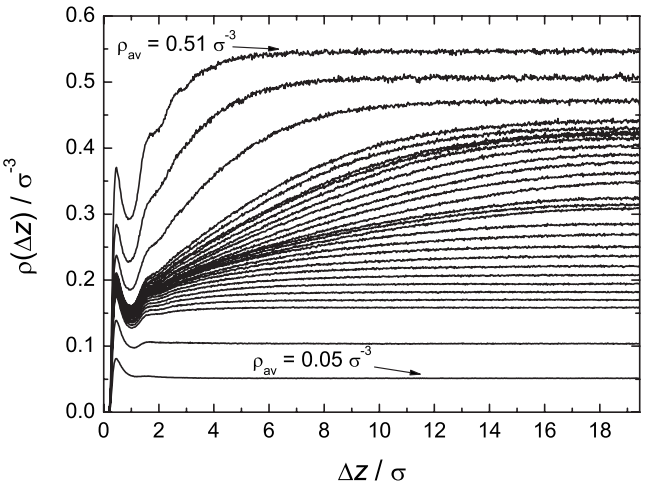


FIG. 8. Selected density profiles $\rho(\Delta z)$ of a LJ fluid in the slit pore with $H=40\sigma$ in the thermodynamic states along the bulk critical isotherm $T=1.1876$.

$\rho(\Delta z)$, represented by Eq. (8) and expected for large $z$.

The values of the correlation length $\xi$ obtained from the fits of $\rho(\Delta z)$ to Eq. (8) are shown in Fig. 10 as a function of the average pore density $\rho_{av}$ and of the density in the pore interior $\rho_{in}$. The values $\rho_{in}$, found from the averaging of the fluid density in the layer of $1\sigma$ width in the pore center, coincide within 0.1% with the values of $\rho_b$ found from the fits of $\rho(\Delta z)$ to Eq. (8). The maximum $\xi$ is observed when the average pore density is $0.278\sigma^{-3}$, which is slightly higher than the pore critical density $0.262\sigma^{-3}$ (dotted line in Fig. 10). In this case, the density in the pore interior is about $0.395\sigma^{-3}$ which is much higher than the critical density $\rho_c^{bulk} \approx 0.325\sigma^{-3}$ of the bulk LJ fluid [31] (dashed line in Fig. 10). The critical isotherm of a LJ fluid confined in the smaller pore of width $H=12\sigma$ was studied in Ref. [31]. The maximal value of the correlation length $\xi$ of about $1.7\sigma$ was

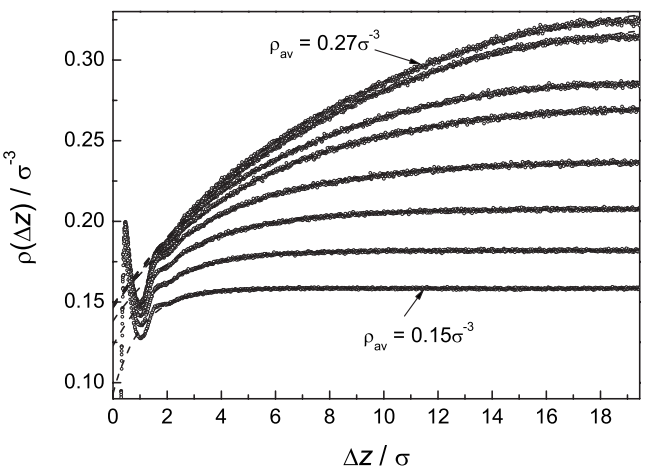


FIG. 9. The density profiles $\rho(\Delta z)$ of a LJ fluid in the slit pore with $H=40\sigma$ along the bulk critical isotherm $T=1.1876$ at some values of the average density $\rho_{av}=0.154$, 0.175, 0.195, 0.216, 0.237, 0.257, 0.262, and $0.267\sigma^{-3}$ (from bottom to top). The fits to the exponential equation (8) in the range $\Delta z \geqslant 2\sigma$ are shown by dashed lines.

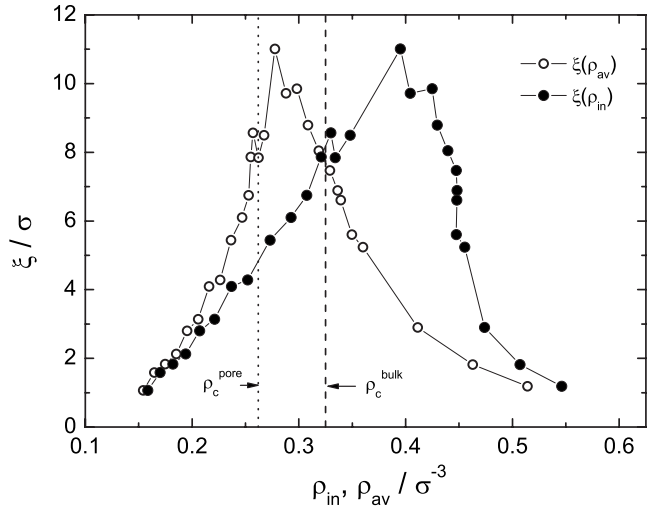


FIG. 10. Correlation length obtained from the fits of the equation (8) to the density profiles $\rho(\Delta z)$ of a LJ fluid in the slit pore with $H=40\sigma$ at the bulk critical isotherm $T=1.1876$ is shown as function of the average pore density $\rho_{av}$ (open circles) and of the density in the pore interior $\rho_{in}$ (solid circles).

observed at $\rho_{av}\approx 0.32\sigma^{-3}$, when the density far from the surface is about $0.42\sigma^{-3}$.

In Fig. 11, we show the relation between the average pore density $\rho_{av}$ and the density $\rho_{in}$ in the pore interior. A solid line $\rho_{in}=\rho_{av}$ corresponds to the absence of the surface effect, when the density profile appears as a slab with the same density through the whole pore. This slab approximation is valid when the correlation length is small, i.e. for low density fluids ($\rho_{in}<0.1\sigma^{-3}$) and for high density fluids ($\rho_{in}\gg 0.5\sigma^{-3}$). The largest difference between $\rho_{in}$ and $\rho_{av}$ is seen at the same densities, where the correlation length is the largest (Fig. 10), thus supporting the idea that the density gradient is governed by the bulk correlation length. The similar relation between $\rho_{in}$ and $\rho_{av}$ is observed in the small pore

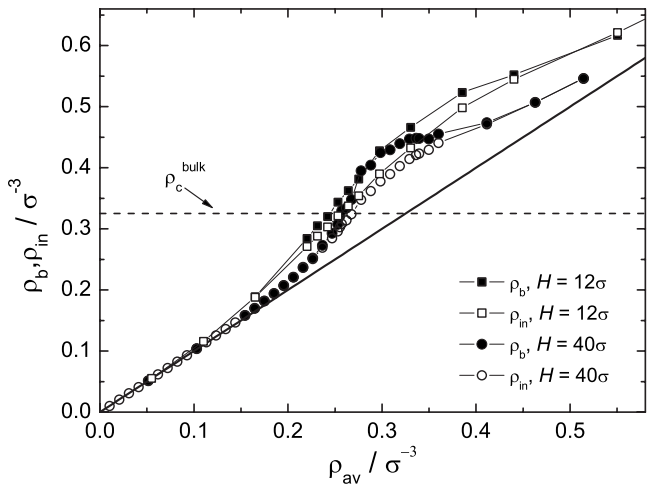


FIG. 11. Relation of the density $\rho_{in}$ in the pore interior and the density $\rho_b$ far away from the surface with the average pore density $\rho_{av}$ along the bulk critical isotherm $T=1.1876$ in pores of width $H=12\sigma$ and $40\sigma$. The function $\rho_{in}$, $\rho_b=\rho_{av}$ is shown by straight solid line.

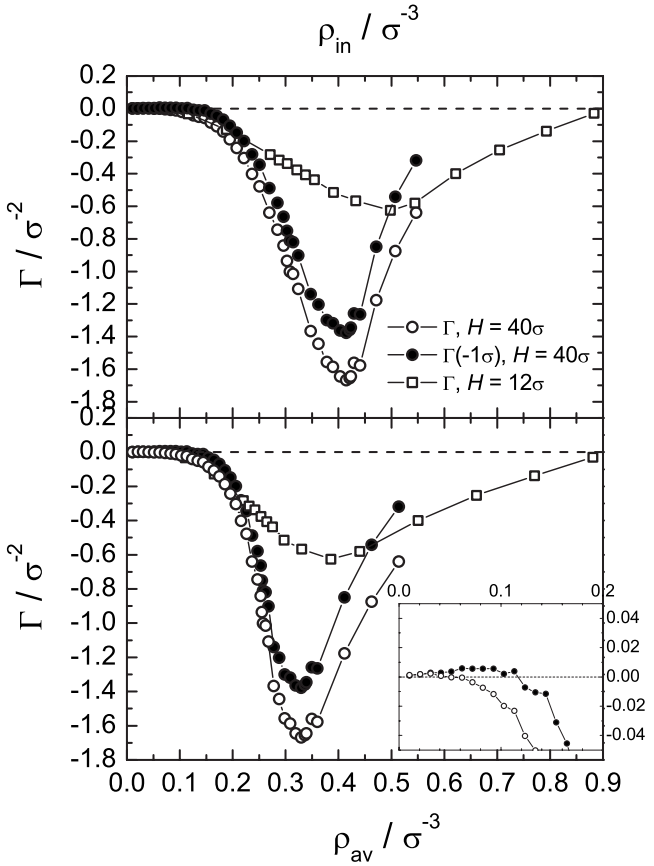


FIG. 12. The excess adsorptions $\Gamma$ and $\Gamma(-1\sigma)$ at the bulk critical isotherm $T=1.1876$ in the pores of width $H=12\sigma$ and $40\sigma$ are shown as a function of the density in the pore interior $\rho_{in}$ (upper panel) and of the average pore density $\rho_{av}$ (lower panel).

of the width $H=12\sigma$, although the critical effect is smeared out in a wider density range (Fig. 11, squares).

The excess adsorption $\Gamma$ of a LJ fluid in various thermodynamic states in both pores along the critical isotherms, calculated by numerical integration of the density profiles using Eq. (12), is shown in Fig. 12 as a function of the average pore density $\rho_{av}$ and of the density $\rho_{in}$ in the pore interior. Minimum value of $\Gamma$ (the largest desorption) is observed at $\rho_{av}=0.329\sigma^{-3}$ and $\rho_{in}=0.414\sigma^{-3}$ in the pore of $40\sigma$ width and $\rho_{av}=0.385\sigma^{-3}$ and $\rho_{in}=0.498\sigma^{-3}$ in the pore of $12\sigma$ width. In both pores, the density in the pore interior notably exceeds the bulk critical density and this effect is stronger in the smaller pore.

## IV. DISCUSSION

### A. Density profiles

A supercritical LJ fluid near a weakly attractive surface shows a strong density depletion in a wide thermodynamic range around the bulk critical point. Such behavior may be treated as an adsorption of voids, whose partial volume increases toward the surface. A negative deviation from the density $\rho_b$ can be well described by Eq. (8), which is Eq. (4) modified for the case of the density depletion, as well as by Eq. (9), which includes asymptotic behaviors not only at

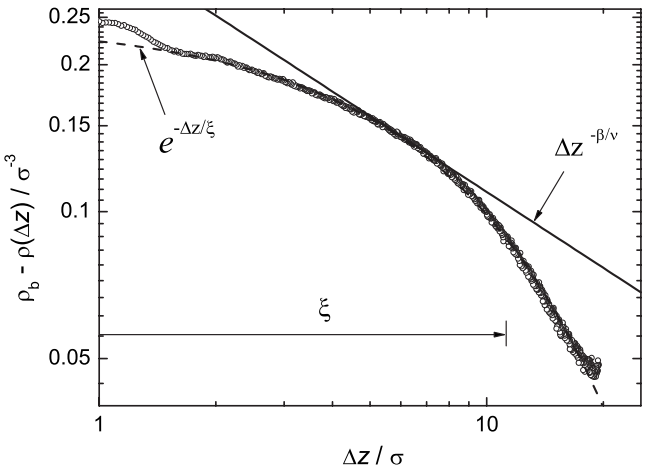


FIG. 13. The density deviation from the bulk value at $T=T_c$ and $\rho_{av}=0.278\sigma^{-3}$ as a function of the distance to the surface in a double logarithmic scale. Fit to the exponential equation (8) is shown by dashed line and a power law (3) is shown by solid line. Distance from the surface equal to the correlation length $\xi$ is shown by arrow.

large but also at small $z$. We have found that both equations yield almost identical perfect fits of $\rho(\Delta z)$, i.e., the similar values of the fitting parameters $\rho_b$ and $\xi$ and the same total mean-square deviation. This observation together with the obtained from the fits an extremely large value of the parameter $c$ in Eq. (9) suggest that the critical contribution $\sim\tau^{-\beta/\nu}$ is negligible in the thermodynamic range studied. This conclusion is illustrated by Fig. 13 for the fluid state, which shows the largest correlation length, $\xi\approx 11\sigma$. Clearly that the whole density profile excluding two density oscillations shows exponential shape not only for $\Delta z>\xi$, but also for $\Delta z<\xi$. Note, that we did not found the expected power law part $\sim\tau^{-\beta/\nu}$ of the order parameter profile for the subcritical LJ fluid in the same pore [28]. Such behavior may be related to the specific nature of the surface field in the case of one component fluid near weakly attractive surfaces. In fact, the effective surface field, which favors voids originates solely from the missing neighbor effect. It is not clear, whether this situation corresponds to the case of a "strong" or "weak" surface field in the case of Ising lattice. We cannot exclude that liquid-vapor coexistence near weakly attractive walls may be mapped onto Ising model only assuming the temperature and density dependent surface field decreasing or vanishing at the critical point. Such specific surface field causes mainly exponential shape of the fluid density profiles and complicates (or prevents) the crossover from the ordinary to normal transition [35], expected close to the critical point for any finite constant surface field in Ising model (see Ref. [36] for more details).

### B. Correlation length

The power law (10) is valid for the correlation length in the thermodynamic states along the bulk critical isochore asymptotically close to the critical temperature. Chemical potential $\mu$ of confined fluid being at the pore critical isochore or at some other isochore with a fixed pore average density changes with temperature in a different way than $\mu$ of bulk fluid at the bulk critical isochore. Nevertheless, the values of the correlation length $\xi$ of confined fluid obtained from the fits of Eq. (8) to the fluid density profiles changes with temperature along the pore critical isochore as well as along another isochore (Fig. 4) in qualitative agreement with Eq. (10). In both cases, the amplitude $\xi_0^+$ in Eq. (10) is close to $0.42\sigma$. This value is about factor of 1.5 of the amplitude $\xi_0^-=0.28\sigma$ found in the same system along the pore coexistence curve. Theoretical as well as experimental studies reveal the ratio $\xi_0^+/\xi_0^-\approx 1.95$ in bulk fluids. The value $\xi_0^-$ has been obtained from the dependence $\xi(\tau)$ along the well-defined thermodynamic path, the coexistence curve, whereas the value $\xi_0^-$ has been obtained from the dependences $\xi(\tau)$ along isochore, which notably differ from the bulk critical one. Therefore, the low value of the ratio $\xi_0^+/\xi_0^-$ should be attributed to the underestimated value of $\xi_0^+$ rather than to the overestimated value of $\xi_0^-$. We may conclude, that deviation of the thermodynamic path corresponding to the pore isochore from the bulk critical isochore causes essential decrease of the amplitude of the correlation length, whereas the temperature dependence $\xi(\tau)$ remains qualitatively the same in a rather wide density range. Slowing down of the dependence $\xi(\tau)$ with respect to the power law (10) when approaching the critical temperature (Fig. 4, lower panel) should be attributed to the increasing effect of the opposite pore wall on the density profile, when $\xi$ exceeds about 13% of the pore width.

At the bulk critical temperature, the correlation length was found larger than $10\sigma$ when the average pore density ($\approx 0.28\sigma^{-3}$) is close but below the bulk critical density, whereas the density in the pore interior is much larger ($\approx 0.40\sigma^{-3}$). In a semi-infinite system, one should expect the strongest density depletion in the case, when the density of a bulk fluid approaches the bulk critical value. However, this is not the case even in a rather large pore. We may conclude, that the chemical potential $\mu$ of a confined fluid is equal to the bulk critical value, when the fluid density in the pore interior notably exceeds the bulk critical density.

### C. Excess adsorption

We have analyzed the excess adsorption $\Gamma$ using numerical integration of the density profiles and assuming the density infinitely far from the surface to be equal the density in the pore center $\rho_{in}$. A three-dimensional diagram of $\Gamma$ in the pore of width $H=40\sigma$ as a function of temperature $T$ and $\rho_{in}$ is shown in Fig. 14. An absolute maximum of desorption $|\Gamma|\approx 1.7\sigma^{-2}$ is located at the critical temperature and $\rho_{in}\approx 0.41\sigma^{-3}$. A gradual decrease of $|\Gamma|$ accompanies any movement away from this thermodynamic state, including the presented thermodynamic paths along the bulk critical isotherm and along the pore isochores. Approaching the critical temperature along the pore critical isochore and along the higher density pore isochore, the excess adsorption $\Gamma$ increases in accordance with the power law $\Gamma\sim\tau^{-\nu}$. This behavior is directly related to the exponential shape of the fluid density profiles. When neglecting the density oscillations, which are notable in the range $\Delta z\leqslant 2\sigma$, the gradual exponential density

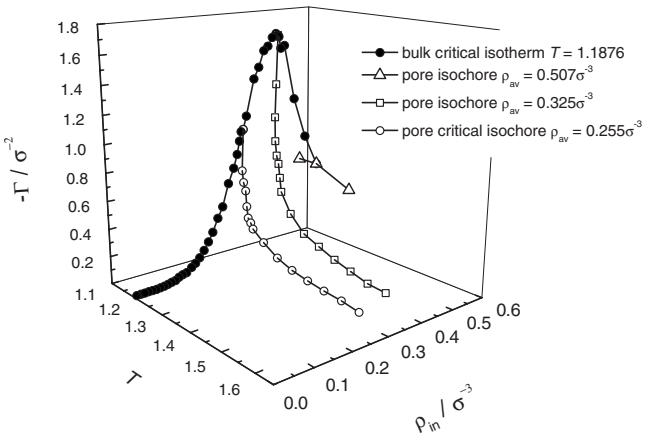


FIG. 14. The excess adsorption $\Gamma$ in the pore with $H=40\sigma$ in the thermodynamic states along the bulk critical isotherm and along the three pore isochores are shown as a function of temperature and of the density $\rho_{\text{in}}$ in the pore interior.

profile, observed at $z>2\sigma$, may be imposed in the whole pore. The gradual excess adsorption $\Gamma_g$ may be calculated by integration of the Eq. (8) from the pore wall to the pore center located at $H^*/2$, so that

$$\Gamma_g = -(\rho_b - \rho_s)\xi\left[1 - \exp\left(-\frac{H^*}{2\xi}\right)\right]. \tag{13}$$

Obviously, the correlation length $\xi$, which diverges at the critical temperature in the bulk fluid, makes a dominant contribution to $\Gamma_g$. In Fig. 15 we compare the density dependence of $\Gamma_g$ in the wide pore $H=40\sigma$ with $\Gamma$ obtained by Eq. (12) using direct numerical integration. The excess desorption $|\Gamma|$ is always smaller than $|\Gamma_g|$ expected from the gradual density profiles. Close to the critical density, $|\Gamma_g|$ exceeds $|\Gamma|$ by about factor of 2. The origin of this discrepancy is the difference between $\rho_{\text{in}}$ and $\rho_b$ in Eqs. (12) and (13), respectively. As it can be seen from in Fig. 11, $\rho_{\text{in}}$ is notably lower

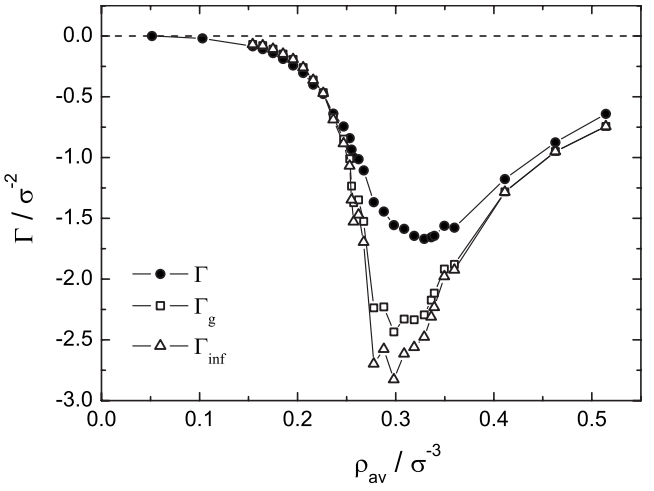


FIG. 15. The excess adsorption $\Gamma$ in the thermodynamic states along the bulk critical isotherm $T=1.1876$ in the pore of width $H=40\sigma$ calculated by Eq. (12) (solid circles), by Eq. (13) (squares), and by Eq. (14) (triangles).

than $\rho_b$ in the density range close to the bulk critical density. This means, that the density $\rho_{\text{in}}$ calculated near a pore center is still affected by the pore wall and can not be identify with the bulk density $\rho_b$ infinitely far from the walls, estimated by the fitting of the fluid density profiles to Eq. (8). Thus, behavior of $\Gamma_g$ is closer to that expected in semi-infinite system. Indeed, extrapolation of Eq. (13) to the semi-infinite system ($H^* \to \infty$) yields excess adsorption $\Gamma_{\text{inf}}$

$$\Gamma_{\text{inf}} = -(\rho_b - \rho_s)\xi, \tag{14}$$

which shows even sharper minimum close to the critical point (see triangles in Fig. 15). Presented analysis evidences, that the density oscillations within two surface layers have a little influence on the excess adsorption in comparison with the gradual exponential shape of the density profiles and they may be neglected in the majority of the practically important situations.

### D. Nonmonotonic behavior of $\Gamma$ and line of zero adsorption

Finally, we discuss a phenomenon observed rather far from the critical point at low densities: a nonmonotonic behavior of $\Gamma$ upon increasing density. Close look on the low-density range (see inset in Fig. 12) evidences an adsorption regime when positive $\Gamma$ increases with increasing density. Eventually, $\Gamma$ passes through a maximum, crosses over to negative values and then passes through the deep minimum in the vicinity of the critical density. Such nonmonotonic behavior with maximum of $\Gamma$ is seen more clearly, when using the excess adsorption $\Gamma(-1\sigma)$ being calculated when the first surface layer is excluded from consideration (open circles in the inset of Fig. 12). The crossover from the adsorption to desorption upon increasing density occurs at $\rho_{\text{in}} \approx \rho_{\text{av}} = 0.120 \pm 0.003\sigma^{-3}$. In a saturated vapor phase, a similar crossover from adsorption to desorption was observed when the density in the pore interior was about $\rho_{\text{in}} \approx \rho_{\text{av}} = 0.115\sigma^{-3}$, indicating that the crossover density may increase upon heating. The possible locations of the line $\Gamma=0$ in the studied system are shown schematically by the dashed and dotted lines in Fig. 16. This line should move to higher densities upon increasing fluid-wall interaction and its temperatures derivative may increase or decrease. However, we can not analyze these trends based on the available simulation data.

For any particular fluid-surface system, there is a line $\Gamma=0$ in the temperature-density plane. Existence of this line is a common phenomena for fluids near surfaces as it reflects competition of the fluid-surface attraction, dominating at low densities, with the effect of missing neighbors, whose importance increases with increasing density [28]. The crossover from adsorption to desorption appears in monotonic decrease of $\Gamma$ with increasing density. On the other hand, the surface perturbation, which determines the absolute value of $\Gamma$, depends on the distance to the critical point in both density (pressure) and temperature coordinates. Therefore, $\Gamma$ should show two extrema when density increases along any (arbitrary) thermodynamic path [37]. In the studied system, first extrema (weak maximum) of $\Gamma$ occurs at very low densities, whereas the second one (strong minimum) occurs close to

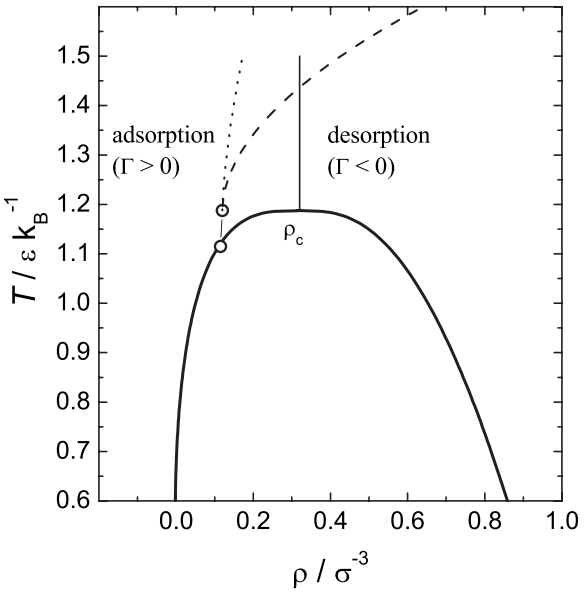


FIG. 16. Crossover from adsorption to desorption occurs when crossing a line of zero excess adsorption $[\Gamma(-1\sigma)=0]$: results of simulations are shown by symbols, their possible extensions to higher temperature are shown by dashed or dotted lines. In the former case, a crossover to excess depletion occurs near the critical temperature upon cooling along the critical isochore (solid line).

the critical point (see Fig. 12). Such behavior has been observed in the simulations of subcritical LJ fluid [28] and of supercritical LJ fluid (present paper). Nonmonotonic crossover of $\Gamma$ from the regime of adsorption to the regime of desorption upon increasing density was recently observed experimentally along supercritical isotherm of propane in aerogel [29]. A crossover density was about 0.25 $g/cm^3$ which is about 54% of the critical density of propane. As the line $\Gamma=0$ should shift to higher densities with the strengthening the fluid-wall attraction, the aerogel should be considered as effectively more adsorptive surface for propane, than the system studied in the present paper.

If the line $\Gamma=0$ shifts to higher densities upon heating, then the crossover from adsorption to desorption should occur when approaching the critical point along the critical isochore. This scenario may be relevant for the experiments [20,23], where pronounced crossover from adsorption to desorption was observed upon cooling along the critical isochore. The steepest negative slope of the line $\Gamma=0$ in the temperature-density plane should occur when the critical point coincides with the crossover point $\Gamma=0$. This corresponds to some particular value of the fluid-wall interaction, which provides practically flat density profiles at the critical point [interaction with $f=0.644$ in Eq. (7) for the considered LJ fluid [27]]. In this case, even small deviations of density from the critical isochore may cause a crossover from strong adsorption to strong desorption. This can be another origin of the drastic crossover from adsorption to desorption seen in experiment [20,23]. Further experimental and simulation studies are necessary to clarify general regularities of the adsorption behavior in supercritical net fluids, related to the nonmonotonic variations of the excess adsorption. The case of the crossover from adsorption to desorption close to the critical density seems to be most intriguing.

## ACKNOWLEDGMENT

Financial support from Deutsche Forschungsgemeinschaft (Grant No. SPP 1155) is gratefully acknowledged.

[1] M. E. Fisher and P.-G. de Gennes, C. R. Seances Acad. Sci., Ser. B **287**, 207 (1978).
[2] R. Guida and J. Zinn-Justin, J. Phys. A **31**, 8103 (1998).
[3] H. Diehl, Ber. Bunsenges. Phys. Chem. **98**, 466 (1994).
[4] M. Smock, H. W. Diehl, and D. P. Landau, Ber. Bunsenges. Phys. Chem. **98**, 486 (1994).
[5] A. J. Liu and M. E. Fisher, Phys. Rev. A **40**, 7202 (1989).
[6] G. Flöter and S. Dietrich, Z. Phys. B: Condens. Matter **97**, 213 (1995).
[7] J. H. Carpenter, J.-H. J. Cho, and B. M. Law, Phys. Rev. E **61**, 532 (2000).
[8] J. Jestin, L.-T. Lee, M. Privat, and G. Zalczer, Eur. Phys. J. B **24**, 541 (2001).
[9] J. R. Howse, E. Manzanares-Papayanopoulos, I. A. McLure, J. Bowers, R. Steitz, and G. H. Findenegg, J. Chem. Phys. **116**, 7177 (2002).
[10] M. Schlossman, X.-L. Wu, and C. Franck, Phys. Rev. B **31**, 1478 (1985).
[11] J. Schulz, J. Bowers, and G. H. Findenegg, J. Phys. Chem. B **105**, 6956 (2001).
[12] J. Bowers, A. Zarbakhsh, A. Querol, H. K. Chistenson, I. A. McLur, and R. Cubitt, J. Chem. Phys. **121**, 9058 (2004).
[13] L. W. Marschand, M. Brown, L. B. Lurio, B. M. Law, S. Uran, I. Kuzmenko, and T. Gog, Phys. Rev. E **72**, 011509 (2005).
[14] U. Ritschel and P. Czerner, Phys. Rev. Lett. **77**, 3645 (1996).
[15] A. Ciach and U. Ritschel, Nucl. Phys. B **489**, 653 (1997).
[16] B. M. Law, Prog. Surf. Sci. **66**, 159 (2001).
[17] A. Ciach, A. Maciolek, and J. Stecki, J. Chem. Phys. **108**, 5913 (1998).
[18] N. S. Desai, S. Peach, and C. Franck, Phys. Rev. E **52**, 4129 (1995).
[19] R. Pini, S. Ottiger, A. Rajendran, G. Storti, and M. Mazzotti, Adsorption **14**, 133 (2008).
[20] M. Thommes, G. Findenegg, and H. Lewandowski, Ber. Bunsenges. Phys. Chem. **98**, 477 (1994).
[21] J. H. Chen, D. S. H. Wong, C. S. Tan, R. Subramanian, C. T. Lira, and M. Orth, Ind. Eng. Chem. Res. **36**, 2808 (1997).
[22] R. Garcia, S. Scheidemantel, K. Knorr, and M. H. W. Chan, Phys. Rev. E **68**, 056111 (2003).
[23] M. Thommes and G. H. Findenegg, Adv. Space Res. **16**, 83 (1995).
[24] M. Schoen, M. Thommes, and G. H. Findenegg, J. Chem. Phys. **107**, 3262 (1997).
[25] A. Maciolek, A. Ciach, and R. Evans, J. Chem. Phys. **108**, 9765 (1998).
[26] A. Maciolek, R. Evans, and N. B. Wilding, Phys. Rev. E **60**,

7105 (1999).
[27] A. Maciolek, R. Evans, and N. B. Wilding, J. Chem. Phys. **119**, 8663 (2003).
[28] A. Oleinikova, I. Brovchenko, and A. Geiger, Eur. Phys. J. B **52**, 507 (2006).
[29] G. Rother, Y. B. Melnichenko, D. R. Cole, H. Frielinghaus, and G. D. Wignall, J. Phys. Chem. C **111**, 15736 (2007).
[30] N. B. Wilding, Phys. Rev. E **52**, 602 (1995).
[31] I. Brovchenko, A. Geiger, and A. Oleinikova, Eur. Phys. J. B **44**, 345 (2005).
[32] A. Oleinikova, I. Brovchenko, and A. Geiger, J. Phys.: Condens. Matter **17**, 7845 (2005).
[33] S. Dietrich, in *Phase Transitions and Critical Phenomena*, edited by C. Domb and J. L. Lebowitz (Academic Press, London, 1988), Vol. 12, pp. 1–218.
[34] U. M. B. Marconi, Phys. Rev. A **38**, 6267 (1988).
[35] H. W. Diehl, in *Phase Transitions and Critical Phenomena*, edited by C. Domb and J. L. Lebowitz (Academic, New York, 1986), Vol. 10, pp. 75–267.
[36] I. Brovchenko and A. Oleinikova, Mol. Phys. **104**, 3535 (2006).
[37] I. Brovchenko and A. Oleinikova, Chem. Unserer Zeit **42**, 152 (2008).